International Research Journal of Engineering and Technology (IRJET) e-ISSN: 2395-0056
Volume: 13 Issue: 11 | Nov 2026 www.irjet.net p-ISSN: 2395-0072

Adaptive Neuro-Fuzzy Control for Solar EV Charging with MPC Comparison

Prakruthi tejasree[1], B. Amarendra Reddy [2]

[1]MTech Student, Department of Electrical Engineering, Andhra University, Andhra Pradesh India
[2]Associate Professor, Department of Electrical Engineering, Andhra University, Andhra Pradesh, India

---

Abstract - *This paper investigates the performance enhancement of an off-grid electric vehicle (EV) charging station powered by photovoltaic (PV) panels and batteries. An adaptive neuro-fuzzy inference system (ANFIS) is employed for maximum power point tracking (MPPT) to improve the utilization of available solar energy. A robust nonlinear control framework is developed for regulating the currents and voltages of the PV, battery, and EV charging system. Conventional sliding mode control (SMC) suffers from chattering, while the super-twisting sliding mode controller (ST-SMC) can experience windup effects under control saturation. To address these limitations, a conditioned-based super-twisting sliding mode controller (CST-SMC) is implemented. The controller gains are optimized using the grey wolf optimization (GWO) algorithm, and system stability is established through Lyapunov analysis. In addition, model predictive control (MPC) is incorporated as a further control strategy for predictive regulation of the power converter and EV charging operation. The complete system, including the PV array, boost converter, DC bus, battery, quadratic buck-boost converter, and EV charger, is modeled and simulated in MATLAB/Simulink. The CST-SMC achieves a rise time of 0.0564 s, overshoot of 0.00389, and settling time of 0.4256 s, compared with 0.137 s, 0.38095, and 3.8071 s, respectively, for ST-SMC. The results demonstrate improved dynamic response and smoother regulation during constant-current and constant-voltage charging stages.*

Key Words: ANFIS, MPPT, Super-twisting sliding mode control, Conditioned-based control, Grey wolf optimization, Quadratic buck-boost converter, Off-grid EV charging station, Model predictive control

1. INTRODUCTION

Electric vehicles (EVs) have gained significant attention due to their potential to reduce air pollution, greenhouse gas emissions, and dependence on conventional fossil fuels [1]–[4]. The integration of renewable energy sources with EV charging infrastructure can further improve the sustainability and energy independence of transportation systems. However, in remote and rural areas where grid connectivity is limited or unavailable, reliable EV charging remains a challenge. Off-grid charging stations powered by renewable energy sources provide a suitable solution by generating and storing electrical energy locally [5], [6].

Among renewable energy sources, photovoltaic (PV) energy is particularly suitable for off-grid EV charging because of its relatively simple energy-conversion structure compared with wind-based systems [7]–[9].

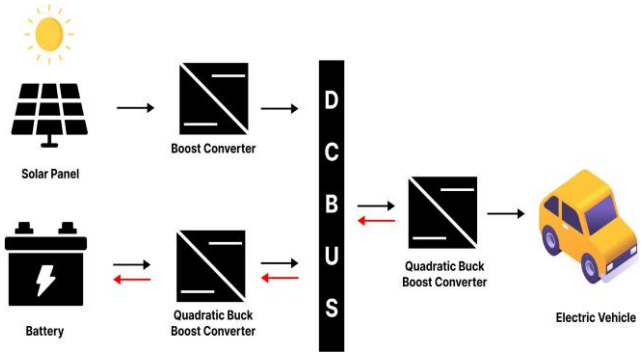

Fig -1: Block diagram of off-grid charging station.

A PV and battery-based charging station can supply energy to EVs during periods of sufficient solar irradiation, while the battery can store excess PV energy and provide backup power when solar generation is insufficient [10]. This combination improves the continuity and reliability of the charging process.

Table -1: Nomenclature.

Abbreviation	Definition
ANFIS	Adaptive neuro-fuzzy inference system
CC	Constant current
CST-SMC	Conditioned-based super-twisting sliding mode control
CV	Constant voltage
DC	Direct current
EV	Electric vehicle
G2V	Grid-to-vehicle
GWO	Grey wolf optimization
KCL	Kirchhoff's current law
MPC	Model predictive control
MPPT	Maximum power point tracking
PV	Photovoltaic
QBBC	Quadratic buck-boost converter
SMC	Sliding mode control
ST-SMC	Super-twisting sliding mode control

Maximum power point tracking (MPPT) is essential for extracting the maximum available power from PV panels under varying irradiation and temperature conditions. Several MPPT techniques, including perturb and observe, incremental conductance, fuzzy logic, and neural-network-based methods, have been investigated to improve PV system efficiency [11], [12]. In this work, an adaptive neuro-fuzzy inference system (ANFIS) is employed for MPPT by combining the learning capability of neural networks with the nonlinear mapping characteristics of fuzzy logic.

The power converters used in renewable-energy-based charging stations have nonlinear dynamics and require effective control techniques for stable voltage and current regulation. A quadratic buck-boost converter (QBBC) provides both step-up and step-down voltage conversion and is therefore suitable for systems with varying input and output voltage requirements [13], [14], [28]. However, its nonlinear behavior makes controller design more challenging.

Several nonlinear control techniques have been developed for PV and battery-based charging systems. Sliding mode control (SMC) provides robustness against system uncertainties and disturbances, but conventional SMC can produce chattering. The super-twisting sliding mode controller (ST-SMC) reduces this chattering problem; however, windup effects can occur when the control input reaches its saturation limit. This work therefore introduces a conditioned-based super-twisting sliding mode controller (CST-SMC) to address this limitation.

Different nonlinear control techniques have been developed for regulating the output voltage of PV systems [15]–[19]. Sliding mode controllers have also been applied to PV and battery-based EV charging stations [20], [21]. However, conventional SMC is associated with chattering and steady-state errors. Super-twisting sliding mode control (ST-SMC) has been investigated for EV charging applications, including Kalman-filter-based charging stations and battery electric vehicles [22], [23].

Despite these developments, several challenges remain in off-grid EV charging systems. The nonlinear characteristics of power converters require robust control techniques for reliable voltage and current regulation. Conventional SMC suffers from chattering and steady-state errors, while ST-SMC may experience windup effects under control saturation. In addition, the integration of optimized control techniques with predictive control for off-grid EV charging systems requires further investigation. Therefore, this work employs a CST-SMC to mitigate windup and control-saturation issues. The system integrates a quadratic buck-boost converter for energy conversion and ANFIS for maximum power point tracking. The controller gains are optimized using the grey wolf optimization (GWO) algorithm [30]. In addition, model predictive control (MPC) is incorporated into the charging system as a further predictive control approach for converter and charging-system regulation. MPC considers the future behavior of the system when generating the control action, which provides an additional framework for regulating converter operation and charging dynamics.

The main contributions of this work are summarized as follows:

- A **CST-SMC** is designed for the PV and battery-based off-grid EV charging station to mitigate windup and control-saturation effects.
- The CST-SMC provides improved dynamic tracking characteristics compared with the conventional ST-SMC.
- Smooth regulation is achieved during the constant-current (CC) and constant-voltage (CV) charging stages.
- **ANFIS-based MPPT** is employed to generate the reference voltage for the PV system.
- The controller gains are optimized using the **grey wolf optimization (GWO)** algorithm, and system stability is established using Lyapunov analysis.
- The proposed control system is evaluated through MATLAB/Simulink simulation.
- MPC is incorporated as an additional predictive control strategy for evaluating the dynamic behavior of the EV charging system.

The remainder of this paper is organized as follows. Section 2 presents the proposed methodology. Section 3 describes the converter topology and mathematical modeling of the system. Section 4 presents the controller design for the PV and battery systems. Section 5 discusses the controller design for the EV charger. Section 6 presents the simulation results, including the MPC implementation. Finally, Section 7 concludes the paper.

2. PROPOSED METHODOLOGY

Fig. 1 illustrates the proposed PV and battery-based off-grid EV charging station. The system utilizes photovoltaic (PV) panels as the primary renewable energy source, while the battery provides energy storage and backup during periods of reduced or unavailable solar irradiation. During sufficient solar generation, the available PV energy is used for EV charging and excess energy can be stored in the battery. During low-solar conditions, the battery supports the charging demand, thereby improving the continuity and reliability of the off-grid charging system.

The proposed system combines ANFIS-based maximum power point tracking (MPPT), robust nonlinear control, and a Model Predictive Control (MPC) strategy. The ANFIS generates the PV reference voltage based on the measured environmental conditions, while the controller regulates

the converter operation to maintain the desired electrical variables. The MPC provides an additional predictive control framework for the converter and charging system.

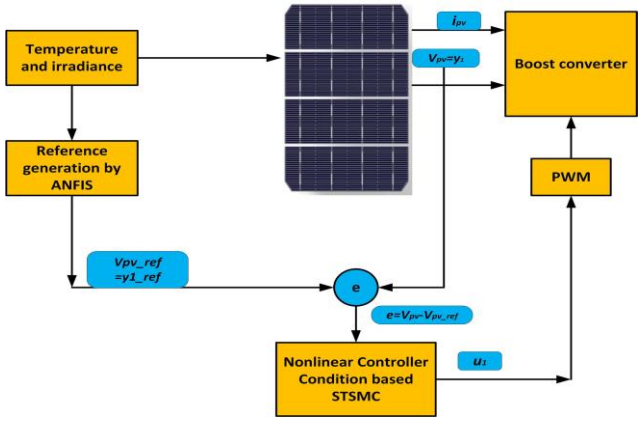

Fig -2: PV reference generation through MPPT.

2.1 PV REFERENCE GENERATION THROUGH ANFIS

ANFIS is employed to generate the reference voltage required for maximum power point tracking of the PV array. It combines fuzzy logic with neural-network learning to represent the nonlinear relationship between the PV operating conditions and the corresponding maximum power point voltage [24]–[27].

The proposed MPPT structure is shown in Fig. 2. The solar irradiance and temperature are measured as inputs to the ANFIS model. Based on these inputs, ANFIS generates the reference PV voltage $V_{pv,ref}$. This reference is compared with the measured PV voltage, and the resulting voltage error is supplied to the nonlinear controller. The controller adjusts the PWM signal of the boost converter to regulate the PV operating voltage around its maximum power point.

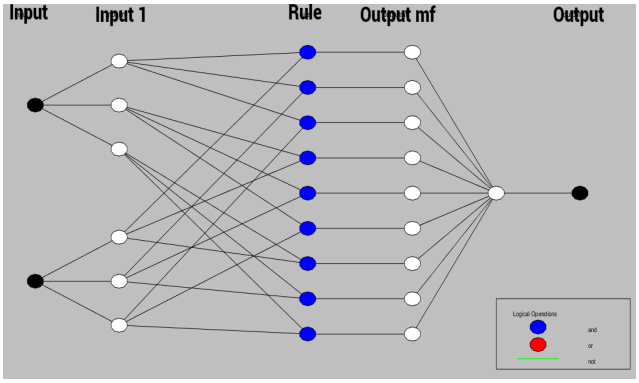

Fig -3: Fuzzy inference system network structure.

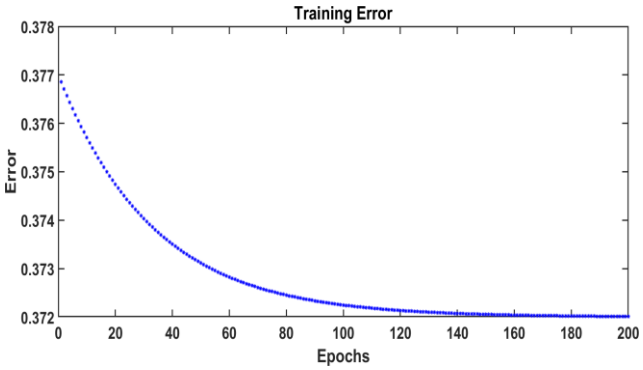

Fig -4: Training error vs. epochs.

The ANFIS structure shown in Fig. 3 consists of input membership functions, fuzzy rules, inference operations, and an output layer. The two inputs are irradiance and temperature, while the output is the reference MPP voltage. The ANFIS model is trained using appropriate PV operating data to establish the nonlinear relationship between the environmental conditions and the reference voltage.

The training error versus the number of epochs is presented in Fig. 4. The training error converges to a small value at approximately 200 epochs, indicating that the ANFIS model successfully learns the required input-output relationship.

2.1.1 Components of the Fuzzy Inference System

The main components of the fuzzy inference system used in the ANFIS model are:

- **Fuzzification:** Converts the measured crisp inputs into corresponding fuzzy variables using membership functions.
- **Rule Base:** Contains IF–THEN rules representing the relationship between irradiance, temperature, and the reference PV voltage.
- **Inference Engine:** Processes the fuzzy rules and determines the corresponding fuzzy output.
- **Defuzzification:** Converts the fuzzy output into a crisp reference voltage value.

In the proposed ANFIS model, triangular membership functions are used for the fuzzification process. The input data may be preprocessed through normalization or scaling before training to improve consistency and training performance.

2.2 MODEL PREDICTIVE CONTROL

Model Predictive Control (MPC) is incorporated into the charging-station control framework. The MPC-based controller uses the system model and measured operating variables to determine appropriate control actions for the

power-converter operation. This provides an additional control approach for evaluating the dynamic behavior of the PV, battery, DC-bus, and EV charging system. The averaged state model of Section 3.1 and the EV-charger model of Section 3.2 can serve as the prediction model for the MPC controller.

[AUTHOR TO COMPLETE: MPC prediction model, cost function, prediction and control horizons, constraints, and control law exactly as implemented in the Simulink model.]

3. MATHEMATICAL MODELING

3.1 MODELING OF CONVERTERS WITH BATTERY AND PV

A quadratic buck-boost converter (QBBC) is employed in the proposed PV and battery-based charging station. As shown in Fig. 5, the QBBC regulates the output voltage v_o by providing step-up or step-down conversion according to the battery input voltage v_{bat}. The converter consists of inductors, capacitors, switches, and diodes.

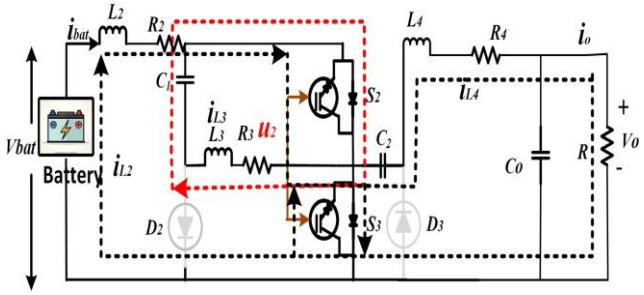

Fig -5: Quadratic buck-boost converter.

3.1.1 MODE 1

During Mode 1, switches S_2 and S_3 are ON, while diodes D_2 and D_3 are reverse biased. As illustrated in Fig. 6, inductors L_2, L_3, and L_4 are energized by the input source and capacitors, while C_1 and C_2 discharge. The PV current i_{pv} through L_1 is driven by the PV voltage v_{pv}, with the resistive loss represented by R_1. Similarly, L_2 is charged through the voltage across C_1, with its resistive loss represented by R_2. The current through switch S_2 is determined by the difference between i_{l2} and i_{l3}. The output capacitor C_o is charged by the current through L_3 while simultaneously supplying the load.

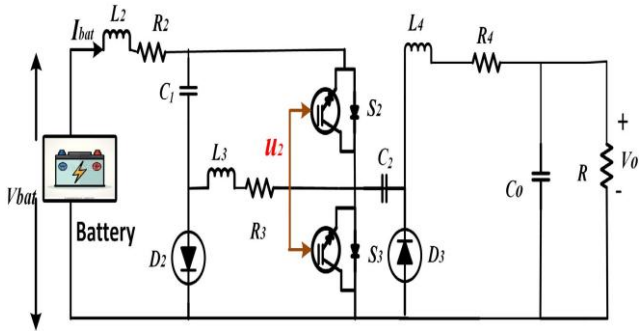

Fig -6: Mode 1.

The dynamic equations for Mode 1 are given by:

$$\frac{di_{pv}}{dt} = \frac{v_{pv}}{L_1} - \frac{R_1}{L_1} i_{pv}$$
$$\frac{di_{bat}}{dt} = \frac{v_{bat}}{L_2} - \frac{R_1}{L_1} i_{bat}$$
$$\frac{di_{l2}}{dt} = \frac{v_{c1}}{L_3} - \frac{R_2}{L_2} i_{l2}$$
$$\frac{di_{l3}}{dt} = \frac{v_{c2}}{L_4} - \frac{R_3}{L_3} i_{l3} - \frac{v_o}{L_3}$$
$$\frac{dv_{c1}}{dt} = \frac{i_{bat}}{C_1}$$
$$\frac{dv_{c2}}{dt} = \frac{i_{l2}}{C_2}$$
$$\frac{dv_{co}}{dt} = \frac{i_{l3}}{C_o} - \frac{v_o}{R}$$

3.1.2 MODE 2

During Mode 2, switches S_2 and S_3 are OFF and diodes D_2 and D_3 conduct. In this mode, the inductors transfer stored energy to the capacitors and output stage. The current i_{pv} decreases because of the opposing capacitor voltage and resistive losses. Similarly, the battery current is affected by the battery voltage and converter resistance. The current through L_2 decreases due to the opposing voltage across C_2, while L_3 transfers energy toward the output capacitor and load.

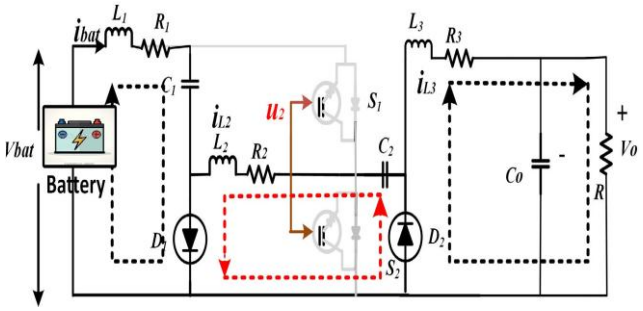

Fig -7: Mode 2.

The corresponding equations are:

$$\begin{aligned}
\frac{di_{pv}}{dt} &= \frac{v_{pv}}{L_1} - \frac{v_{c1}}{L_1} - \frac{R_1}{L_1} i_{pv} \\
\frac{di_{bat}}{dt} &= \frac{v_{bat}}{L_2} - \frac{R_2}{L_2} i_{bat} \\
\frac{di_{l2}}{dt} &= -\frac{v_{c2}}{L_2} - \frac{R_2}{L_2} i_{l2} \\
\frac{di_{l3}}{dt} &= -\frac{R_3}{L_3} i_{l3} - \frac{v_o}{L_3} \\
\frac{dv_{c1}}{dt} &= \frac{i_{bat}}{C_1} \\
\frac{dv_{c2}}{dt} &= \frac{i_{l2}}{C_2} \\
\frac{dv_{co}}{dt} &= \frac{i_{l3}}{C_o} - \frac{v_o}{R}
\end{aligned}$$

3.1.3 AVERAGED MODEL OF THE QBBC

The averaged model of the converter is obtained by applying the inductor volt-second balance and capacitor charge balance over one switching period. The resulting equations are:

$$\frac{di_{pv}}{dt} = \frac{v_{pv}}{L_1} - \frac{R_1}{L_1} i_{pv} - \frac{1-u_1}{L_1} v_{co} \quad (1)$$

$$\frac{di_{bat}}{dt} = \frac{v_{bat}}{L_2} - \frac{R_2}{L_2} i_{bat} - \frac{1-u_2}{L_2} v_{c1} \quad (2)$$

$$\frac{di_{l2}}{dt} = \frac{v_{c1}}{L_2} - \frac{R_2}{L_2} i_{bat} - \frac{1-u_2}{L_2} v_{c2} \quad (3)$$

$$\frac{di_{l3}}{dt} = \frac{v_{c2}}{L_3} u_2 - \frac{R_3}{L_3} i_{l3} - \frac{v_o}{L_3} \quad (4)$$

$$\frac{dv_{c1}}{dt} = \frac{i_{bat}}{C_1}(1-u_2) - \frac{i_{l2}}{C_1} u_2 \quad (5)$$

$$\frac{dv_{c2}}{dt} = -\frac{i_{l2}}{C_2}(1-u_2) + \frac{i_{bat}}{C_2}(1-u_2) \quad (6)$$

$$\frac{dv_{co}}{dt} = -\frac{i_{l3}}{C_o} - \frac{i_o}{C_o} \quad (7)$$

These equations represent the averaged dynamic model of the QBBC over one switching period.

3.1.4 STATE-SPACE REPRESENTATION

For controller design, the averaged variables are represented using the state variables y_1–y_{10} and control inputs u_1, u_2, and u_3:

$$\begin{aligned}
y_1 &= \langle i_{pv} \rangle,\ y_2 = \langle i_{bat} \rangle,\ y_3 = \langle i_{l2} \rangle, \\
y_4 &= \langle i_{l3} \rangle,\ y_5 = \langle v_{c1} \rangle,\ y_6 = \langle v_{c2} \rangle, \\
y_7 &= \langle v_{co} \rangle,\ y_8 = \langle i_L \rangle,\ y_9 = \langle v_{bat} \rangle, \\
y_{10} &= \langle v_c \rangle.
\end{aligned}$$

The control variables are represented as

$$u_1 = \langle u_1 \rangle,\ u_2 = \langle u_2 \rangle,\ u_3 = \langle u_3 \rangle.$$

$$\dot{y}_1 = \frac{v_{pv}}{L_1} - \frac{R_1}{L_1} i_{pv} - \frac{1-u_1}{L_1} v_{co} \quad (8)$$

$$\dot{y}_2 = \frac{v_{bat}}{L_2} - \frac{R_2}{L_2} i_{bat} - \frac{1-u_2}{L_2} v_{c1} \quad (9)$$

$$\dot{y}_3 = \frac{v_{c1}}{L_2} u_2 - \frac{R_2}{L_2} i_{bat} - \frac{1-u_2}{L_2} v_{c2} \quad (10)$$

$$\dot{y}_4 = \frac{v_{c2}}{L_3} u_2 - \frac{R_3}{L_3} i_{l3} - \frac{v_o}{L_3} \quad (11)$$

$$\dot{y}_5 = \frac{i_{bat}}{C_1}(1-u_2) - \frac{I_{L2}}{C_1} u_2 \quad (12)$$

$$\dot{y}_6 = -\frac{i_{l2}}{C_2}(1-u_2) + \frac{i_{bat}}{C_2}(1-u_2) \quad (13)$$

$$\dot{y}_7 = -\frac{i_{l3}}{C_o} - \frac{i_o}{C_o} \quad (14)$$

The resulting averaged state model is used for the ST-SMC and CST-SMC controller design and can also serve as the prediction model for the MPC controller.

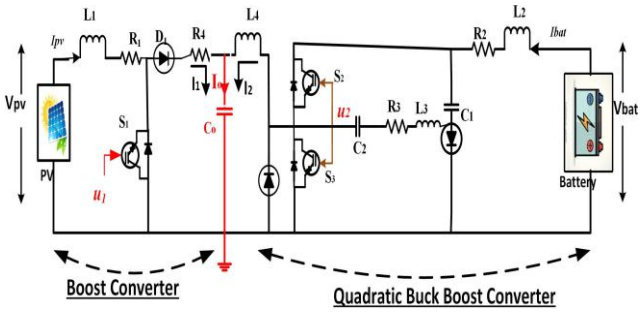

Fig -8: Circuit diagram of charging station.

3.2 MODELING OF EV CHARGER

An off-board EV charger is incorporated into the proposed off-grid charging station. As shown in Fig. 9, the charger consists of a DC–DC quadratic buck-boost converter coupled with a Thevenin equivalent battery model on the load side. The power converter includes two IGBTs, S_4 and S_5, inductors L_5, L_6, and L_7, diodes D_4 and D_5, and capacitors C_3 and C_4.

The Thevenin battery model consists of a capacitor C_{bat} and equivalent resistive elements. The series resistance R_s represents the equivalent resistance associated with the battery plates, electrolyte, and conductors, whereas the parallel resistance R_p represents the equivalent leakage effects within the battery. This model is used to represent the electrical behavior of the EV battery during the charging process.

Here, y_8, y_9, and y_{10} represent the inductor current, battery outer voltage, and battery internal voltage, respectively.

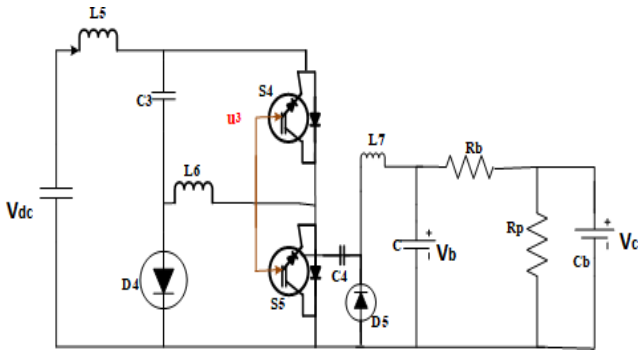

Fig -9: EV charger model.

The dynamic equations of the EV charger are given by:

$$\dot{y}_8 = -\frac{y_9}{L_7} + \frac{u_3 v_{dc}}{L_7} \qquad (15)$$

$$\dot{y}_9 = \frac{1}{C} y_8 - \frac{1}{R_s C} y_9 + \frac{1}{R_s C} y_{10} \qquad (16)$$

$$\dot{y}_{10} = \frac{1}{R_s C_{bat}} y_9 - \frac{1}{R_s C_{bat}} y_{10} - \frac{1}{R_p C_{bat}} y_{10} \qquad (17)$$

[AUTHOR TO CONFIRM: Eq. (17) was corrupted in the supplied file and has been restored by analogy with Eq. (16). Verify it against the source model.]

4. CONTROLLER DESIGN

In this work, Super-Twisting Sliding Mode Control (ST-SMC) and Conditioned-Based Super-Twisting Sliding Mode Control (CST-SMC) are designed for accurate reference-current tracking in the PV and battery systems. The battery acts as the primary energy source, while the PV system provides supplementary power. ST-SMC improves tracking performance in the nonlinear charging system; however, control saturation may lead to windup effects. The conditioned-based approach introduces an additional conditioning mechanism to improve the control response under saturation and achieve smoother current tracking.

The power balance of the charging station is expressed as

$$P_{in} = P_L \qquad (18)$$

where P_{in} is the total input power supplied by the PV and battery systems and P_L is the load power required by the EV charger. The input power can be expressed as

$$P_{in} = P_{bat} + P_{pv} \qquad (19)$$

where P_{bat} and P_{pv} represent the battery and PV power, respectively.

By substituting the corresponding power expressions into (19), the battery reference current is obtained as

$$I_{batref} = \zeta\left(\frac{V_{dc} i_L - v_{pv} I_{pvref}}{v_{bat}}\right) \qquad (20)$$

where ζ represents the ideality factor associated with the power losses in the converters due to inductive, resistive, and switching effects.

4.1 SUPER-TWISTING SLIDING MODE CONTROL

The tracking errors for the PV and battery reference currents are defined as

$$e_1 = y_1 - y_{1ref} \qquad (21)$$

$$e_2 = y_2 - y_{2ref} \qquad (22)$$

where y_{1ref} and y_{2ref} are the reference currents of the PV and battery systems, respectively.

Differentiating (21) and (22) with respect to time and substituting the corresponding converter-state equations gives

$$\dot{e}_1 = \frac{v_{pv}}{L_1} - \frac{R_1}{L_1} i_{pv} - \frac{y_7}{L_1}(1 - u_1) - \dot{y}_{1ref} \qquad (23)$$

and

$$\dot{e}_2 = \frac{v_{bat}}{L_2} - \frac{R_2}{L_2} i_{bat} - \frac{y_4}{L_2}(1 - u_2) - \dot{y}_{2ref}. \qquad (24)$$

The sliding surfaces are defined as

$$S_i = a_i e_i,\ i = 1,2 \qquad (25)$$

where a_i is a positive design parameter. Therefore,

$$\dot{S}_1 = a_1\left(\frac{v_{pv}}{L_1} - \frac{R_1}{L_1} i_{pv} - \frac{y_7}{L_1}(1-u_1) - \dot{y}_{1ref}\right) \quad (26)$$

$$\dot{S}_2 = a_2\left(\frac{v_{bat}}{L_2} - \frac{R_2}{L_2} i_{bat} - \frac{y_4}{L_2}(1-u_2) - \dot{y}_{2ref}\right). \quad (27)$$

For stability analysis, the Lyapunov function is selected as

$$V = \sum_{i=1}^{2} \frac{1}{2} S_i^2. \quad (28)$$

Its time derivative is

$$\dot{V} = \sum_{i=1}^{2} S_i \dot{S}_i. \quad (29)$$

The reaching law for the super-twisting sliding mode controller is defined as

$$\dot{S}_i = -k_i \mid S_i \mid^{\alpha_i} \operatorname{sign}\left(\frac{S_i}{\phi}\right) + u_{sw} \quad (30)$$

where k_i is the controller gain, α_i is a positive design parameter between 0 and 1, ϕ is introduced to reduce chattering, and u_{sw} represents the super-twisting control component.

where $i = 1,2$, α_i is a positive real number between 0 and 1, and ϕ is introduced to reduce the chattering effect. The controller parameter k_i is a positive design parameter. The super-twisting control component u_{sw} is defined as

$$u_{sw} = -k_3 \int \operatorname{sign}(S_i)\, dt \quad (31)$$

Substituting the sliding surface defined in (25) into the reaching law in (30) and equating it with the derivative of the sliding surface gives

$$-k_i \mid S_i \mid^{\alpha_i} \operatorname{sign}\left(\frac{S_i}{\phi}\right) - k_3 \int \operatorname{sign}(S_i)\, dt = a_i \dot{e}_i. \quad (32)$$

By substituting the error dynamics given in (23) and (24) into (32) and solving for the control inputs, the control laws for the PV and battery converters are obtained as

$$u_1 = \frac{L_1}{a_1 y_7}\left[\frac{a_1 R_1}{L_1} i_{pv} - \frac{a_1 v_{pv}}{L_1} + \frac{a_1 y_7}{L_1} - a_1 \dot{y}_{1ref} - k_1 \mid S_1 \mid^{\alpha_1} \operatorname{sign}\left(\frac{S_1}{\phi}\right) - k_3 \int \operatorname{sign}(S_1)\, dt\right] \quad (33)$$

and

$$u_2 = \frac{L_2}{a_2 y_4}\left[\frac{a_2 R_2}{L_2} i_{bat} - \frac{a_2 v_{bat}}{L_2} + \frac{a_2 y_4}{L_2} - a_2 \dot{y}_{2ref} - k_2 \mid S_2 \mid^{\alpha_2} \operatorname{sign}\left(\frac{S_2}{\phi}\right) - k_3 \int \operatorname{sign}(S_2)\, dt\right]. \quad (34)$$

4.2 CONDITIONED-BASED ST-SMC

To overcome the windup and control-saturation problems associated with conventional ST-SMC, the conditioned-based ST-SMC introduces an additional conditioning variable v_i. The reaching law is defined as

$$\dot{S}_i = -k_i \mid S_i \mid^{\alpha_i} \operatorname{sign}\left(\frac{S_i}{\phi}\right) + u_{sw} - v_i. \quad (35)$$

The conditioning variable v_i is defined as

$$v_i = m_i \int \operatorname{sign}(u_{tsat} - v_i)\, dt \quad (36)$$

where m_i is a positive design parameter. The saturated control input u_{tsat} is constrained by the maximum control limit P, which is expressed as

$$u_{tsat} = \begin{cases} u_t, & \mid u_t \mid \leq P \\ P \operatorname{sign}(u_t), & \mid u_t \mid > P \end{cases} \quad (37)$$

Substituting the sliding surface from (25) into the conditioned reaching law and using the super-twisting component gives

$$-k_i \mid S_i \mid^{\alpha_i} \operatorname{sign}\left(\frac{S_i}{\phi}\right) - k_3 \int \operatorname{sign}(S_i)\, dt - v_i = a_i \dot{e}_i. \quad (38)$$

Using the error dynamics in (23) and (24), the corresponding control inputs are obtained as

$$u_1 = \frac{L_1}{a_1 y_7}\left[\frac{a_1 R_1}{L_1} i_{pv} - \frac{a_1 v_{pv}}{L_1} + \frac{a_1 y_7}{L_1} - a_1 \dot{y}_{1ref} - k_1 \mid S_1 \mid^{\alpha_1} \operatorname{sign}\left(\frac{S_1}{\phi}\right) - k_3 \int \operatorname{sign}(S_1)\, dt - v_1\right] \quad (39)$$

$$u_2 = \frac{L_2}{a_2 y_4}\left[\frac{a_2 R_2}{L_2} i_{bat} - \frac{a_2 v_{bat}}{L_2} + \frac{a_2 y_4}{L_2} - a_2 \dot{y}_{2ref} - k_2 \mid S_2 \mid^{\alpha_2} \operatorname{sign}\left(\frac{S_2}{\phi}\right) - k_3 \int \operatorname{sign}(S_2)\, dt - v_2\right]. \quad (40)$$

The conditioned-based formulation introduces v_i into the control law to account for the effect of actuator saturation and thereby reduce the windup effect. This is the key difference between the conventional ST-SMC and CST-SMC formulations in the paper.

5. CONTROLLER DESIGN FOR BATTERY ELECTRIC VEHICLE CHARGER

Conditioned-based Super-Twisting Sliding Mode Control (CST-SMC) and Super-Twisting Sliding Mode Control (ST-SMC) are designed to regulate the battery charging process through the proposed charging station. The Grid-to-Vehicle (G2V) operating mode corresponds to the charging of the EV battery from the charging station. In the G2V mode, both constant-current (CC) and constant-voltage (CV) charging modes are considered [23], [29].

5.1 SUPER-TWISTING SLIDING MODE CONTROL

By applying Kirchhoff's Current Law (KCL), the battery current i_{bat} can be expressed as

$$i_{bat} = \frac{y_8 - y_9}{C} \quad (41)$$

where y_8, y_9, and C represent the corresponding state variables and capacitance of the EV charger model.

The battery-current tracking error is defined as

$$e_3 = i_{bat} - i_{batref} \quad (42)$$

where i_{batref} represents the desired reference value of the battery charging current.

The other two error terms are defined as

$$e_4 = y_9 - y_{9ref} \quad (43)$$

$$e_5 = y_{10} - y_{10ref} \quad (44)$$

where y_{9ref} and y_{10ref} are the desired reference values associated with the capacitor voltages.

By differentiating (42)–(44) with respect to time, and considering the reference values i_{batref}, y_{9ref}, and y_{10ref} as constant, the error dynamics are obtained as

$$\dot{e}_3 = \frac{\dot{y}_8 - \dot{y}_9}{C} \quad (45)$$

$$\dot{e}_4 = \dot{y}_9 \quad (46)$$

$$\dot{e}_5 = \dot{y}_{10} \quad (47)$$

The sliding surface for the EV battery charger is then defined as

$$\dot{S}_3 = a_3 \dot{e}_3 + a_4 \dot{e}_4 + a_5 \dot{e}_5 \quad (48)$$

where a_3, a_4, and a_5 are positive design parameters.

By applying the super-twisting reaching law given in (32), the following expression is obtained:

$$-k_3 \mid S_3 \mid^{\alpha_3} \operatorname{sign}\left(\frac{S_3}{\phi}\right) - k_3 \int \operatorname{sign}(S_3)\, dt = a_3 \frac{\dot{y}_8 - \dot{y}_9}{C} + a_4 \dot{y}_9 + a_5 \dot{y}_{10} \quad (49)$$

From (49), the control input u_3 can be calculated as

$$u_3 = -\frac{L_7}{a_3 v_{dc}}\left(-y_9 a_3 + a_4 \dot{y}_9 + a_5 \dot{y}_{10} + k_3 \mid S_3 \mid^{\alpha_3} \operatorname{sign}\left(\frac{S_3}{\phi}\right) + k_3 \int \operatorname{sign}(S_3)\, dt\right) \quad (50)$$

where u_3 represents the control input associated with the EV charger converter.

5.2 CONDITIONED-BASED ST-SMC

For the conditioned-based super-twisting sliding mode controller, the reaching law in (35) is equated with the sliding-surface dynamics in (49). This gives

$$a_3 \frac{\dot{y}_8 - \dot{y}_9}{C} + a_4 \dot{y}_9 + a_5 \dot{y}_{10} = -k_3 \mid S_3 \mid^{\alpha_3} \operatorname{sign}\left(\frac{S_3}{\phi}\right) - k_3 \int \operatorname{sign}(S_3)\, dt - v_3 \quad (51)$$

where v_3 is the conditioning term introduced to handle the effect of control saturation and reduce windup.

Substituting the error dynamics from (45)–(47) into (51), the following expression is obtained:

$$a_3 \dot{e}_3 + a_4 \dot{e}_4 + a_5 \dot{e}_5 = -k_3 \mid S_3 \mid^{\alpha_3} \operatorname{sign}\left(\frac{S_3}{\phi}\right) - k_3 \int \operatorname{sign}(S_3)\, dt - v_3 \quad (52)$$

By substituting the expression for y_8 from (15) into (52) and solving for the control input u_3, the conditioned-based control law is obtained as

$$u_3 = -\frac{L_7}{a_3 v_{dc}}(-y_9 a_3 + a_4 \dot{y}_9 + a_5 \dot{y}_{10} + k_3 \mid S_3 \mid^{\alpha_3} \operatorname{sign}\left(\frac{S_3}{\phi}\right) + k_3 \int \operatorname{sign}(S_3)\, dt + v_3) \quad (53)$$

The additional v_3 term provides the conditioning mechanism for the EV charger controller. It modifies the control action when saturation occurs and is therefore used to mitigate the windup effect associated with the super-twisting controller.

6. SIMULATION RESULTS

6.1 PERFORMANCE OF ST-SMC AND CST-SMC

The performance of the ST-SMC and CST-SMC controllers is evaluated in MATLAB/Simulink under a stepped load-current demand and varying solar irradiance. The simulation results are shown in Fig. 10. The DC bus voltage is regulated at its reference value, and the PV and battery currents track their references with CST-SMC responding faster than ST-SMC. Table 2 summarizes the dynamic response of the two controllers.

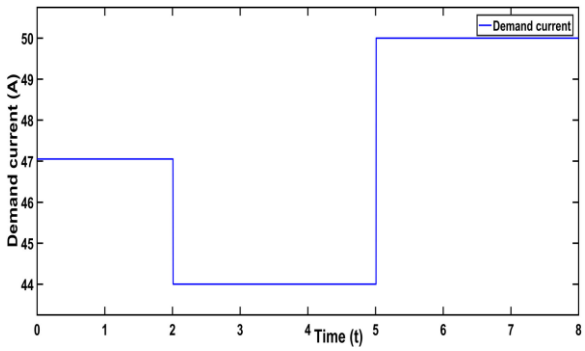

(a) Load current

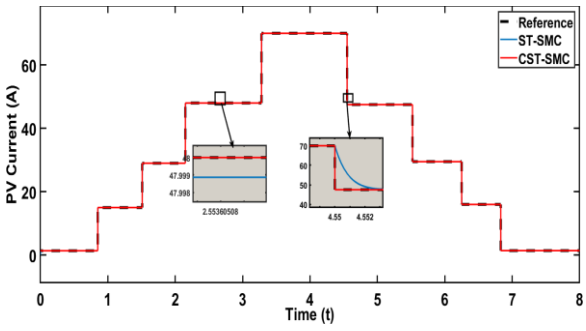

(b) PV current

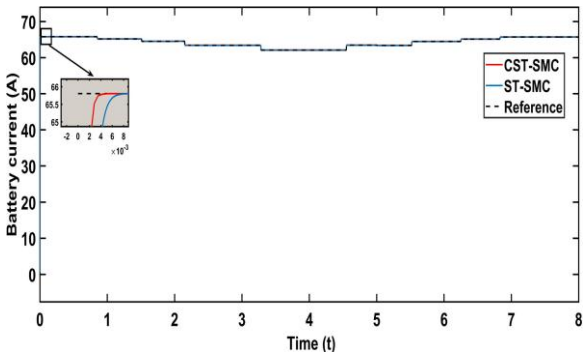

(c) Battery current

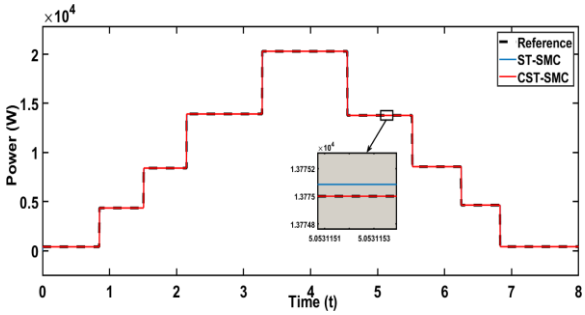

(d) PV power

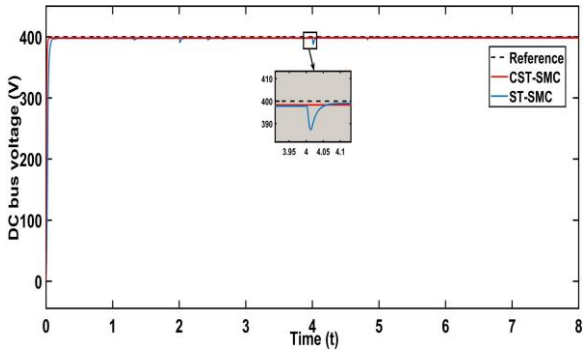

(e) DC bus voltage

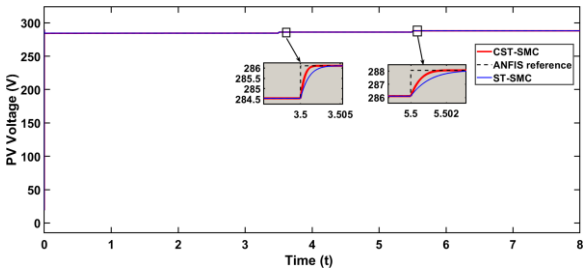

(f) Effect of irradiance on PV voltage

Fig -10: Simulation results of ST-SMC and CST-SMC for [a] load current, [b] PV current, [c] battery current, [d] PV power, [e] DC bus voltage and [f] effect of irradiance on PV voltage.

Table -2: Dynamic response of ST-SMC and CST-SMC.

Controller	Rise time (s)	Overshoot	Settling time (s)
ST-SMC	0.137	0.38095	3.8071
CST-SMC	0.0564	0.00389	0.4256

6.2 PERFORMANCE OF THE MPC EXTENSION

The MPC controller uses the mathematical model of the converter and EV charger to predict the future behavior of the system and determine the corresponding control action. The resulting responses are shown in Fig. 11.

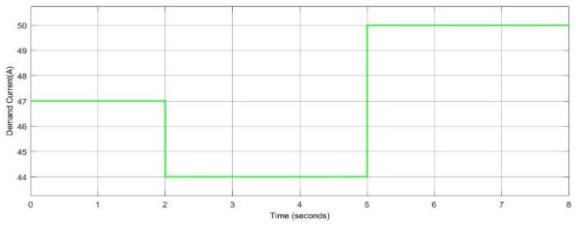

(a) Load current

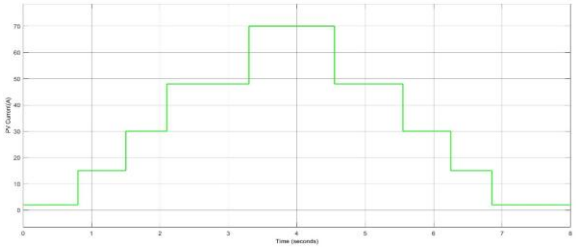

(b) PV current

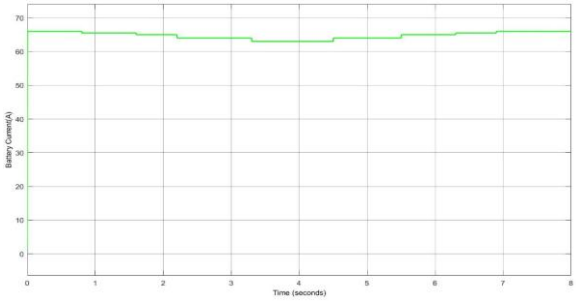

(c) Battery current

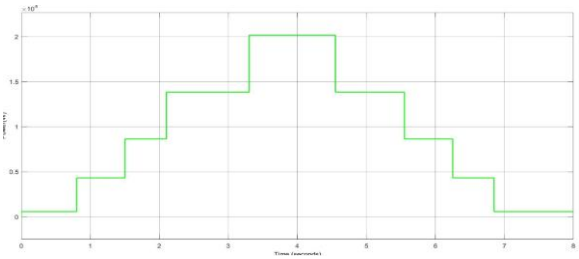

(d) PV power

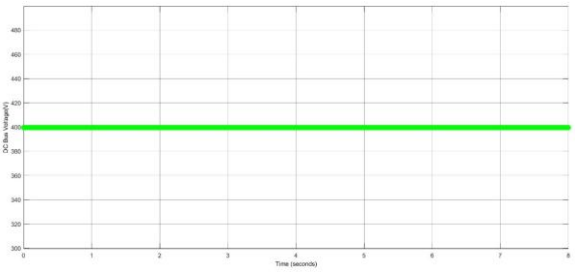

(e) DC bus voltage

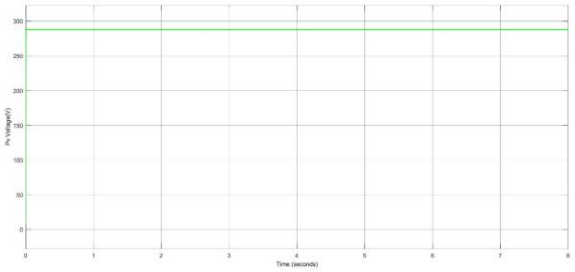

(f) Effect of irradiance on PV voltage

Fig -11: Simulation results of the MPC for [a] load current, [b] PV current, [c] battery current, [d] PV power, [e] DC bus voltage and [f] effect of irradiance on PV voltage.

[AUTHOR TO COMPLETE: quantitative MPC results (rise time, settling time, overshoot, steady-state error, charging-current ripple) and comparison with ST-SMC and CST-SMC.]

7. CONCLUSIONS

A battery and PV-based off-grid EV charging station incorporating a quadratic buck-boost converter has been modeled and investigated. The proposed charging station enables effective utilization of available solar energy while the battery provides energy storage to support continuous system operation. The reference peak voltage for PV maximum power point tracking (MPPT) is generated using an adaptive neuro-fuzzy inference system (ANFIS).

The Grey Wolf Optimization (GWO) algorithm is employed to optimize the controller gains. The simulation results demonstrate that the conditioned-based super-twisting sliding mode controller (CST-SMC) provides improved tracking performance compared with the conventional super-twisting sliding mode controller (ST-SMC), particularly in terms of steady-state error and chattering reduction. The robustness of the proposed controller is evaluated under variations in the operating conditions, including changes in solar irradiance.

Model Predictive Control (MPC) is additionally incorporated into the charging station model as a predictive control strategy for regulating the converter and

EV charging operation by considering the future behavior of the system.

Despite the improvements achieved through the proposed control framework, the performance of the off-grid charging station can be affected by variations in environmental conditions, particularly solar irradiance and temperature. In addition, battery energy management, capacity degradation, and lifetime remain important considerations for long-term operation.

Future work can focus on developing advanced energy-management strategies for multiple charging stations, investigating different battery technologies and hybrid energy-storage systems, and further optimizing controller parameters using advanced optimization techniques such as Whale Optimization Algorithm (WOA) and Red Wolf Optimization (RWO). Further investigation of the proposed MPC strategy under different charging and environmental conditions can also be considered.

REFERENCES

1) F. Jelti, A. Allouhi, K. Anissa, and T. Aoul, "Transition paths towards a sustainable transportation system: A literature review," Sustainability, vol. 15, no. 21, 2023, Art. no. 15457.

2) J. Tang, X. Xiao, M. Han, R. Shan, D. Gu, T. Hu, G. Li, P. Rao, N. Zhang, and J. Lu, "China's sustainable energy transition path to low-carbon renewable infrastructure manufacturing under green trade barriers," Sustainability, vol. 16, no. 8, p. 3387, Apr. 2024.

3) F. Liu, M. Shafique, and X. Luo, "Literature review on life cycle assessment of transportation alternative fuels," Environ. Technol. Innov., vol. 32, Nov. 2023, Art. no. 103343, doi: 10.1016/j.eti.2023.103343.

4) B. T. Gul, S. H. Ahmed, I. Ahmad, and O. Zeb, "Optimized barrier-condition nonlinear control of wireless charger-based hybrid electric vehicle," J. Energy Storage, vol. 97, Sep. 2024, Art. no. 112705.

5) V. Kumar, V. R. Teja, M. Singh, and S. Mishra, "PV based off-grid charging station for electric vehicle," IFAC-PapersOnLine, vol. 52, no. 4, pp. 276–281, 2019, doi: 10.1016/j.ifacol.2019.08.211.

6) A. Al Wahedi and Y. Bicer, "Development of an off-grid electrical vehicle charging station hybridized with renewables including battery cooling system and multiple energy storage units," Energy Rep., vol. 6, pp. 2006–2021, Nov. 2020, doi: 10.1016/j.egyr.2020.07.022.

7) R. T. Kumar and C. C. A. Rajan, "Integration of hybrid PV-wind system for electric vehicle charging: Towards a sustainable future," e-Prime-Adv. Electr. Eng., Electron. Energy, vol. 6, Dec. 2023, Art. no. 100347, doi: 10.1016/j.prime.2023.100347.

8) J. Gowardhan, S. Ghotekar, and S. Thomas, "Hybrid solar-wind charging station for electric vehicles and its simulation," Int. J. Res. Appl. Sci. Eng. Technol., vol. 10, no. 8, pp. 1780–1783, Aug. 2022.

9) L. Farah, A. Hussain, A. Kerrouche, C. Ieracitano, J. Ahmad, and M. Mahmud, "A highly-efficient fuzzy-based controller with high reduction inputs and membership functions for a grid-connected photovoltaic system," IEEE Access, vol. 8, pp. 163225–163237, 2020.

10) U. Datta, A. Kalam, and J. Shi, "Smart control of BESS in PV integrated EV charging station for reducing transformer overloading and providing battery-to-grid service," J. Energy Storage, vol. 28, Apr. 2020, Art. no. 101224, doi: 10.1016/j.est.2020.101224.

11) P. K. Pathak, S. Padmanaban, A. K. Yadav, P. A. Alvi, and B. Khan, "Modified incremental conductance MPPT algorithm for SPV-based grid-tied and stand-alone systems," IET Gener., Transmiss. Distrib., vol. 16, no. 4, pp. 776–791, Feb. 2022.

12) O. Zeb, B. T. Gul, and I. Ahmad, "Nonlinear MPPT algorithm for PV system using a condition based supertwisting sliding mode control and artificial neural networks," in Proc. 20th Int. Bhurban Conf. Appl. Sci. Technol. (IBCAST), Aug. 2023, pp. 167–176.

13) A. Sarikhani, B. Allahverdinejad, M. Hamzeh, and E. Afjei, "A continuous input and output current quadratic buck-boost converter with positive output voltage for photovoltaic applications," Sol. Energy, vol. 188, pp. 19–27, Aug. 2019, doi: 10.1016/j.solener.2019.05.025.

14) M. Kumar, K. P. Panda, R. T. Naayagi, R. Thakur, and G. Panda, "A critical analysis of quadratic boost based high-gain converters for electric vehicle applications: A review," Sensors, vol. 24, no. 7, p. 2186, Mar. 2024.

15) S. H. Hanzaei, S. A. Gorji, and M. Ektesabi, "A scheme-based review of MPPT techniques with respect to input variables including solar irradiance and PV arrays' temperature," IEEE Access, vol. 8, pp. 182229–182239, 2020.

16) S. Ahmed, H. M. M. Adil, I. Ahmad, M. K. Azeem, Z. E. Huma, and S. A. Khan, "Supertwisting sliding mode algorithm based nonlinear MPPT control for a solar PV

system with artificial neural networks based reference generation," Energies, vol. 13, no. 14, p. 3695, Jul. 2020.

17) V. Kumar and M. Singh, "Derated mode of power generation in PV system using modified perturb and observe MPPT algorithm," J. Modern Power Syst. Clean Energy, vol. 9, no. 5, pp. 1183–1192, Sep. 2021.

18) V. D. Sagias, P. Zacharia, A. Tempeloudis, and C. Stergiou, "Adaptive neuro-fuzzy inference system-based predictive modeling of mechanical properties in additive manufacturing," Machines, vol. 12, no. 8, p. 523, Jul. 2024.

19) M. T. Mitsuya and A. A. de Moura Meneses, "Efficiency of hybrid MPPT techniques based on ANN and PSO for photovoltaic systems under partially shading conditions," Amer. J. Eng. Appl. Sci., vol. 12, no. 4, pp. 460–471, Apr. 2019.

20) S. Ghosh, A. K. Singh, A. K. Paul, and S. N. Singh, "Disturbance observer-based sliding mode control of PV-battery assisted EV charging station," in Proc. IEEE 8th Uttar Pradesh Sect. Int. Conf. Electr., Electron. Comput. Eng. (UPCON), Nov. 2021, pp. 1–6.

21) D. Mazumdar, P. K. Biswas, C. Sain, and T. S. Ustun, "GAO optimized sliding mode based reconfigurable step size Pb&O MPPT controller with grid integrated EV charging station," IEEE Access, vol. 12, pp. 10608–10620, 2024.

22) D. Çelik, H. Ahmed, and M. E. Meral, "Kalman filter-based super-twisting sliding mode control of shunt active power filter for electric vehicle charging station applications," IEEE Trans. Power Del., vol. 38, no. 2, pp. 1097–1107, Apr. 2023.

23) I. Ahmed, I. Ahmad, S. Ahmed, and H. M. M. Adil, "Robust nonlinear control of battery electric vehicle charger in grid to vehicle applications," J. Energy Storage, vol. 42, Oct. 2021, Art. no. 103039, doi: 10.1016/j.est.2021.103039.

24) S. R. Revathy, V. Kirubakaran, M. Rajeshwaran, T. Balasundaram, V. Sekar, S. Alghamdi, B. S. Rajab, A. O. Babalghith, and E. M. Anbese, "Design and analysis of ANFIS-based MPPT method for solar photovoltaic applications," Int. J. Photoenergy, vol. 2022, pp. 1–9, May 2022.

25) K. Amara, A. Fekik, D. Hocine, M. L. Bakir, E.-B. Bourennane, T. A. Malek, and A. Malek, "Improved performance of a PV solar panel with adaptive neuro fuzzy inference system ANFIS based MPPT," in Proc. 7th Int. Conf. Renew. Energy Res. Appl. (ICRERA), Oct. 2018, pp. 1098–1101.

26) N. Priyadarshi, S. Padmanaban, J. B. Holm-Nielsen, F. Blaabjerg, and M. S. Bhaskar, "An experimental estimation of hybrid ANFIS–PSO-based MPPT for PV grid integration under fluctuating sun irradiance," IEEE Syst. J., vol. 14, no. 1, pp. 1218–1229, Mar. 2020.

27) M. R. Javed, A. Waleed, U. S. Virk, and S. Z. U. Hassan, "Comparison of the adaptive neural-fuzzy interface system (ANFIS) based solar maximum power point tracking (MPPT) with other solar MPPT methods," in Proc. IEEE 23rd Int. Multitopic Conf. (INMIC), Nov. 2020, pp. 1–5.

28) M. Okati, M. Eslami, and B. Khan, "A novel semi-quadratic buck-boost structures with continuous input current for PV application," Sci. Rep., vol. 14, no. 1, Jun. 2024, Art. no. 14134.

29) I. Ahmed, H. M. M. Adil, S. Ahmed, I. Ahmad, and Z. Rehman, "Robust nonlinear control of battery electric vehicle charger in grid to vehicle and vehicle to grid applications," J. Energy Storage, vol. 52, Aug. 2022, Art. no. 104813, doi: 10.1016/j.est.2022.104813.

30) S. Mirjalili, S. M. Mirjalili, and A. Lewis, "Grey wolf optimizer," Adv. Eng. Softw., vol. 69, pp. 46–61, Mar. 2014, doi: 10.1016/j.advengsoft.2013.12.007.